The Effects of Climate Change on
Tradeoffs Among Forest Ecosystem Services

Nicholas D. C. Kullman

A thesis
submitted in partial fulfillment of the
requirements for the degree of

Master of Science

University of Washington

2016

Committee:

Sándor F. Tóth, Chair

David Butman

W. Art Chaovalitwongse

Program Authorized to Offer Degree:
Quantitative Ecology and Resource Management

University of Washington

Abstract

The Effects of Climate Change on
Tradeoffs Among Forest Ecosystem Services

Nicholas D. C. Kullman

Chair of the Supervisory Committee:
Associate Professor Sándor F. Tóth
School of Environmental and Forest Sciences

DRAFT

Forests provide a bounty to humans through ecosystem services such as wildlife habitat, recreation, and water and air purification. Forest managers seek to maximize the provision of ecosystem services and often do so for multiple ecosystem services simultaneously. While many studies predict that climate change will impact forests' ability to provide ecosystem services, no research has addressed the question of how climate change will impact the joint provision of ecosystem services. I address this question here in an attempt to better understand how the relationships between ecosystem services will change with climate. For example, how much additional fire hazard must be assumed in order to maintain an amount of habitat for a particular species. To study this question, I consider the growth of a forested area in the Deschutes National Forest under three climate scenarios of varying intensity. This area provides three competing ecosystem services whose joint provision is assessed under each of the climate scenarios: northern spotted owl habitat, water quality, and resistance to wildfire.

I find that . . .

TABLE OF CONTENTS

LIST OF FIGURES

LIST OF TABLES

GLOSSARY

CLIMATE PROJECTION: The IPCC defines a climate projection as a model-derived estimate of future climate. *See* CLIMATE SCENARIO[57].

CLIMATE SCENARIO: The IPCC defines a scenario as a coherent, internally consistent and plausible description of a possible future state of the world. Herein, I use this term interchangeably with CLIMATE PROJECTION, since climate projections often underlie climate scenarios [57].

CLUSTER: Here, a set of contiguous forest stands whose combined area exceeds 200 ha

ECOSYSTEM SERVICE: Benefits that people receive from ecosystems, divided into four categories: supporting, provisioning, regulating and cultural [5]. Examples include food, soil formation, water purification, carbon storage, recreation, and education.

PARETO EFFICIENT: A solution to a multi-objective mathematical program is said to be Pareto efficient if no component of the solution can be improved without compromising at least one other component.

STAND DENSITY INDEX (SDI): Reineke's Stand Density Index is a measure of the stocking of a forest stand. See [62].

TRADEOFF: The sacrifice of achievement in one objective in order to achieve more in another.

ACKNOWLEDGMENTS

DRAFT

Thank you to all who contributed to my earning this degree.

DEDICATION

DRAFT

To ma femme and my family

Chapter 1

MEASURING CONFLICT IN MULTI-OBJECTIVE OPTIMIZATION: A CASE STUDY OF THE IMPACT OF CLIMATE CHANGE ON THE JOINT PROVISION OF FOREST ECOSYSTEM SERVICES

1.1 Introduction

Many tasks in resource allocation are multi-objective. The design of aircraft involves balancing cost and efficiency [79]. Hospitals seek to manage personnel and equipment in order to maximize patient throughput while minimizing cost and required back-up [38]. Food production balances processing time with nutrient retention [68]. Forest managers aim to provide carbon sequestration and wildlife habitat while also maximizing timber revenues [75].

Given a set of solutions to one of these resource allocation problems, a decision maker chooses one to enact. Often, no one solution simultaneously optimizes all objectives, and the decision maker must therefore choose a solution that represents a preferred compromise among them. In such cases, there is some amount of conflict among the objectives. This is in contrast to compatible or harmonious objective relationships in which the objectives improve simultaneously.

In the case of aircraft design, cost and efficiency conflict with one another, since more efficient design details tend to cost more. Similarly, hospitals may increase patient throughput by increasing the number of doctors available, but this decision would increase costs. Food production engineers can maximize nutrient retention by reducing the temperature at which processing occurs, but this would lengthen the time required to reach acceptable microbiological levels. Forest managers can maximize timber revenue by removing large old-growth timber, but this would reduce the available wildlife habitat.

While the preferred solution may vary by decision maker, a rational decision maker will prefer one which is Pareto efficient; that is, a solution in which no objective can be improved without compromising another. Multi-objective optimization affords the knowledge of such solutions and can help guide the decision maker by revealing where objectives can be achieved simultaneously and where they conflict. Having access to the set of Pareto efficient solutions may also help the decision maker locate solutions where compromises in one objective allow outweighing improvements in another. For instance the forest manager may discover that forgoing small amounts of timber revenues allows for the sequestration of significantly more carbon. Or the hospital may be able to increase patient throughput substantially if they hire one additional oncologist. Regardless of whether a decision maker selects a solution providing such gains, the awareness of these relationships enables more informed decision making.

In addition to studying conflict within a system, we may further consider the situation in which a decision maker oversees multiple systems, each with its own set of Pareto efficient solutions. This could be the case for a manager overseeing multiple hospitals or multiple food processing facilities. Alternatively, each system could correspond to a different scenario, such as a forest manager analyzing resource allocation under various realizations of climate change. In such instances, understanding the changes in the conflict relationships between systems may benefit the decision maker, allowing them to ask questions such as: How does the relationship between carbon sequestration and timber revenues vary under different climate change scenarios? Do all hospitals require the same increase in cost to increase patient throughput?

To date, the multi-objective optimization literature has not addressed conflict in these system-level questions. We do so for the first time here, laying a foundation for quantitative conflict analysis. To perform this investigation, we draw on measures commonly used in the field of evolutionary multi-objective optimization (EMO), including various Pareto set indicators and correlation measures. Researchers in EMO use the Pareto set indicators to measure the performance of algorithms that approximate the optimal Pareto set [84];

the correlation measures are used as an aid to increase the computational tractability of the multi-objective problems encountered in EMO [9]. Here we adapt these measures to better study conflicting management objectives across systems. We also develop a new metric for quantifying the conflict between a pair of objectives. The new pairwise conflict metric developed here improves on other commonly used pairwise conflict metrics such as the Pearson and Spearman coefficients. Unlike any current metric, the one we propose can capture mutual objective achievement and accurately identify the lack of conflict between objectives. We demonstrate the novel utility of the existing and proposed conflict metrics on a multi-objective scenario-based case study in the Deschutes National Forest.

In the upcoming sections, we first define terminology. Then we detail the case study and present its results including the application of the new and existing metrics. We conclude with a summary and suggestions for future research.

1.2   Methods

We lay a foundation for quantitative conflict analysis of multi-objective systems. The analysis involves the use of measures that include existing indicators of frontier performance used in EMO, adaptations of indicators used in EMO, and a new measure of conflict that we introduce for the first time here. A case study on the impacts of climate change on forest management serves to illustrate the conflict analysis. Prior to describing the case study, we first define terminology and describe each of the measures used in our analysis.

1.2.1   Terminology

The multi-objective problem   Consider the M-objective optimization problem

Maximize

$$\mathbf{f} = [f_1(\mathbf{x}), f_2(\mathbf{x}), \ldots, f_M(\mathbf{x})] \tag{1.1}$$

subject to

$$\mathbf{x} \in X \tag{1.2}$$

with *objective functions* $f_i(\mathbf{x}), i \in \{1, \dots, M\}$ and feasible *decision vectors* (or *solutions*) $\mathbf{x} \in \mathbb{R}^n$ where n is the number of decision variables in the optimization problem. A set of equality and inequality constraints determine the *feasible decision space X*. Solutions in X are referenced by superscripts: $X = \{\mathbf{x}^1, \mathbf{x}^2, \dots, \mathbf{x}^{|X|}\}$. Each objective function $f_i : \mathbb{R}^n \mapsto \mathbb{R}$ maps decision vectors to scalars in $\mathbb{R}$. The vector objective function $\mathbf{f} : X \mapsto \mathbb{R}^M$ maps the feasible decision space to the *objective space $\mathbb{R}^M$*. The set of all objective functions is the *objective set $\mathcal{M} = \{f_1, \dots, f_M\}$*.

Dominance and frontiers A solution $\mathbf{x}^1$ is said to *dominate* another solution $\mathbf{x}^2$ ($\mathbf{x}^1 \succ \mathbf{x}^2$) if

$$\exists f_i \in \mathcal{M} : f_i(\mathbf{x}^1) > f_i(\mathbf{x}^2) \text{ and } \forall f_i \in \mathcal{M} \ f_i(\mathbf{x}^1) \geq f_i(\mathbf{x}^2) \tag{1.3}$$

A solution $\mathbf{x}^1 \in X$ is *non-dominated* if

$$\nexists \mathbf{x}^2 \in X : \mathbf{x}^2 \succ \mathbf{x}^1 \tag{1.4}$$

For a rational decision maker, all dominated solutions may be removed from the analysis, since for a dominated solution $\mathbf{x}^2$ there exists another solution $\mathbf{x}^1$ which is better: $\mathbf{x}^1$ achieves more in at least one objective than $\mathbf{x}^2$, and $\mathbf{x}^1$ does not achieve less in any objective than $\mathbf{x}^2$. Thus, the decision maker will always select a solution from the set of non-dominated decision vectors that solve the multi-objective problem (1.1) and (1.2). We refer to this set as the *Pareto-optimal set $P = \{\mathbf{x} \in X | \nexists \mathbf{y} \in X : \mathbf{y} \succ \mathbf{x}\}$*.

The *Pareto-optimal frontier*, the *efficient frontier* or, simply, the *frontier Z* is the corresponding set of M-dimensional *objective vectors* $\mathbf{z} = [f_1(\mathbf{x}), f_2(\mathbf{x}), \dots, f_M(\mathbf{x})]$. That is,

$$Z = \{\mathbf{z} = [f_1(\mathbf{x}), \dots, f_M(\mathbf{x})] \mid \mathbf{x} \in P\} \tag{1.5}$$

Objective vectors' components are referred to in subscripts:

$$\mathbf{z} = [z_1, z_2, \dots, z_M] \tag{1.6}$$

Objective vectors provide the decision maker with knowledge of the objective achievement of a solution $\mathbf{x}$ - the ith component of an objective vector $\mathbf{z}$ represents the achievement in objective i by the corresponding decision vector $\mathbf{x}$.

Ideal and nadir objective vectors The *ideal objective vector* is defined as the vector

$$\mathbf{z}^{\text{ideal}} = \max_{\mathbf{x} \in X}\{f_i(\mathbf{x})\} \quad \forall i \in \mathcal{M}. \tag{1.7}$$

Analogously, define the nadir solution as the vector

$$\mathbf{z}^{\text{nadir}} = \min_{\mathbf{x} \in X}\{f_i(\mathbf{x})\} \quad \forall i \in \mathcal{M}. \tag{1.8}$$

The ideal objective vector represents the impossible ideal scenario in which each objective is simultaneously optimized. The nadir objective vector represents the worst case scenario in which each objective attains its lowest value. These solutions are the diagonal corners of the minimum bounding box for the efficient frontier Z. Since they provide upper and lower bounds for each objective, they serve as reference points against which the decision maker can compare solutions.

Trade-offs The *trade-off* between two objective vectors $\mathbf{z}^1$ and $\mathbf{z}^2$ is the vector of differences in their objective achievements:

$$\tau^{1,2} = [z_1^2 - z_1^1, z_2^2 - z_2^1, \ldots, z_M^2 - z_M^1] \tag{1.9}$$

The components of $\tau^{1,2}$ represent the amount of each objective that would be sacrificed or gained by selecting $\mathbf{z}^2$ instead of $\mathbf{z}^1$. Note that $\tau^{1,2} = -\tau^{2,1}$.

Sub-dimensions During analysis, we often wish to consider only a subset of the objectives $\mathcal{L} \subset \mathcal{M}$. We define such subsets as *sub-dimensional objective sets*. In these cases, it is simpler to work with constructs that have only those components that correspond to the objectives in $\mathcal{L}$. For instance, define the *sub-dimensional objective vector* for the solution $\mathbf{x}^i$ as $\mathbf{z}_{\mathcal{L}}^i$ which has components $\forall \ell \in \mathcal{L}. z_\ell^i = f_\ell(\mathbf{x}^i)$. Define the *sub-dimensional trade-off* $\tau_{\mathcal{L}}^{1,2}$ as the vector with components $\forall \ell \in \mathcal{L}. \tau_\ell^{1,2}$.

Relative objective achievements, relative objective vectors, and relative trade-offs   Using the nadir and ideal objective vectors, we can represent each solution as a vector of its relative objective achievements. This allows for dimensionless and scale-agnostic comparison of solutions. For an objective vector $\mathbf{z}$, its *relative achievement in objective i* is

$$\overline{z}_i = \frac{z_i - z_i^{\text{nadir}}}{z_i^{\text{ideal}} - z_i^{\text{nadir}}}, \tag{1.10}$$

and the corresponding *relative objective vector* is

$$\overline{\mathbf{z}} = [\overline{z_1}, \overline{z_2}, \ldots, \overline{z_M}]. \tag{1.11}$$

For two objective vectors $\mathbf{z}^1$ and $\mathbf{z}^2$, the corresponding *relative trade-off* is

$$\overline{\tau}^{1,2} = \left[\overline{z_1^2} - \overline{z_1^1}, \overline{z_2^2} - \overline{z_2^1}, \ldots, \overline{z_M^2} - \overline{z_M^1}\right] \tag{1.12}$$

Conflict, monotonicity, bundles and stacks   We use the following test to determine if Objectives in an objective set $\mathcal{L}$ *do not conflict* if the objectives improve simultaneously: $\forall \mathbf{z}^1, \mathbf{z}^2 \in Z, i \in \mathcal{L}$

$$(z_i^1 \geq z_i^2) \Rightarrow (z_j^1 \geq z_j^2) \quad \forall j \in \mathcal{L}, j \neq i \tag{1.13}$$

If (1.13) does not hold, then the objectives conflict. Any pair of objectives $i, j \in \mathcal{M}$ such that equation (1.13) holds are said to *increase monotonically*. In the case of monotonically increasing objectives i and j, improving objective i also yields improvement in objective j. Conversely, if

$$(z_i^1 \geq z_i^2) \Rightarrow (z_j^1 \leq z_j^2) \quad \forall \mathbf{z}^1, \mathbf{z}^2 \in Z, j \neq i \tag{1.14}$$

holds, then objectives i and j are said to *decrease monotonically*.

When the objectives represent goods or services, a set of objectives that conflict is defined as a *bundle* and a set of objectives that do not conflict is defined as a *stack*.

Equation (1.13) checks for monotonically increasing relationships among objectives. This means of detecting conflict is functionally equivalent to that used by many studies, such as Brockhoff and Zitzler (2009) [10] and Purshouse and Fleming (2003) [60].

1.2.2   Conflict metrics

Given an efficient frontier, the decision maker will determine which solution represents the best compromise among the objectives. Knowledge of the conflicts among the objectives enables better decision making, as it may highlight areas of the efficient frontier where objectives are incompatible and areas where advantageous compromises may exist. To help a decision maker understand the total conflict in the multi-objective system, we employ the hypervolume indicator, which measures the percentage of the objective space bounded by the frontier. The hypervolume indicator maps an efficient frontier to a scalar value representing conflict. However, the scalar value provided by the indicator does not provide the decision maker with detail about where the conflict exists within a multi-objective system. To address this question, we developed a new metric that quantifies the conflict between a pair of objectives, allowing the decision maker to determine from which objective pair does the conflict indicated by the hypervolume indicator originate.

When a decision maker has more than one multi-objective system to analyze, they require a means of comparing the efficient frontiers. To make this comparison, we use the binary hypervolume indicator. The metric is similar to its non-binary counterpart mentioned above, except it maps two efficient frontiers to a scalar. That is, it provides a value for each pair of frontiers, rather than for each frontier individually.

We describe each of these metrics in more detail here.

Hypervolume Indicators   The hypervolume indicator measures the proportional volume of the objective space bounded by the frontier. We use this to measure conflict because systems with conflicting objectives that inhibit the achievement of one another will produce solutions that do not simultaneously achieve in all of the objectives. This results in solutions whose extension into the objective space is limited, which produces a smaller value for the hypervolume.

For each relative objective vector $\overline{\mathbf{z}}^i$ in the frontier Z, define its corresponding hyperrectangle by r_i. r_i is the M-orthotope which has as a pair of diagonally opposite points the

origin and the point defined by the components of the relative objective vector $\overline{\mathbf{z}^i}$. Then the hypervolume indicator is the volume of the union of these hyperrectangles r_i:

$$I_{H1}(Z) = \text{vol}\left(\bigcup_{i=1}^{|Z|} r_i\right) \tag{1.15}$$

Then we can define the *binary hypervolume indicator* of two frontiers Z^1 and Z^2 as [83]

$$I_{H2}(Z^1, Z^2) = I_{H1}(Z^1 + Z^2) - I_{H1}(Z^2) \tag{1.16}$$

where $I_{H1}(Z^1 + Z^2)$ is the unary hypervolume indicator of the frontier that consists of the nondominated points in $\{Z^1 \cup Z^2\}$. See Figure C.3.

We use the binary hypervolume indicator to determine the volume of the objective space that is bounded by frontier Z^1 but not frontier Z^2. Values of $I_{H2}(Z^1, Z^2) > 0$ indicate areas of the objective space bound only by Z^1, implying the presence of regions of less conflict among the objectives. See Figure C.3.
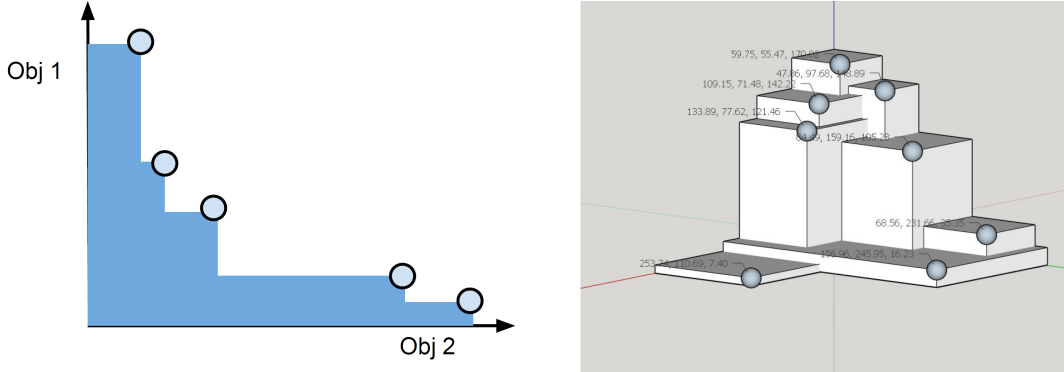

Figure 1.1: Depiction of the hypervolumes of frontiers with two objectives (left) and three objectives (right).

We developed a custom algorithm to compute the hypervolume indicator. The algorithm begins with a list of the relative objective vectors, denoted in the algorithm simply by $\mathbf{z} \in Z$. These vectors are assumed to be sorted in descending order based on their mth
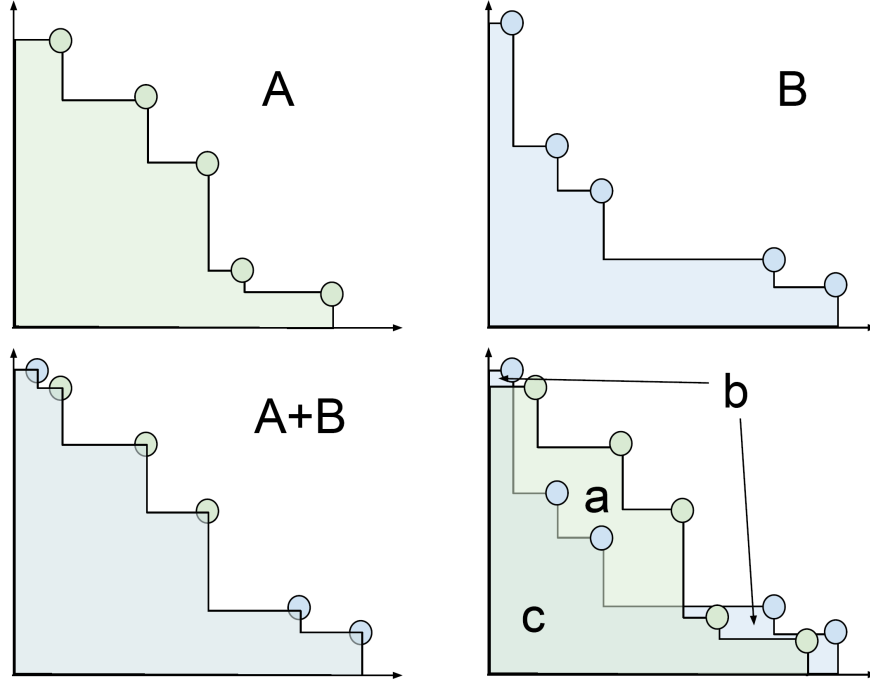
Figure 1.2: Depiction of the binary hypervolume indicator. The individual frontiers are shown in the top row: frontier A (left) and frontier B (right). The merged frontier $A + B$ is shown in bottom left - note the absence of points that were dominated when combined. Following the naming of regions as shown in the bottom right figure, the binary hypervolume indicator is equal to

$$I_{H2}(A, B) = (\text{area}_a + \text{area}_b + \text{area}_c) - (\text{area}_b + \text{area}_c) = \text{area}_a$$

component, for some arbitrary objective $m \in \mathcal{M}$. We define the sub-dimensional objective set $\mathcal{L} = \mathcal{M} \backslash \{m\}$ whose cardinality we denote by $|\mathcal{L}| = L = M - 1$.

We initialize the algorithm with an empty set of non-dominated solutions in L dimensions, G. Let the volume of this nondominated set be denoted $\overline{V}$. We sequentially add solutions from Z to G, adding at each iteration the contribution of the solution $\mathbf{z}$ to the hypervolume indicator V. These contributions are computed by multiplying the solution's mth component z_m by its contribution to the volume of G, $\overline{V}_{\mathbf{z}}$. See Figure 1.3 for reference ($\overline{V}_{\mathbf{z}}$ values are the areas of the yellow regions).

$\overline{V}_{\mathbf{z}}$ is computed as follows. Initialize $\overline{V}_{\mathbf{z}} = 0$ and add $\mathbf{z}$ to G. Remove from G any

solutions that are dominated by $\mathbf{z}$ in L dimensions. Add to $\overline{V}_{\mathbf{z}}$ the value of the volume of $\mathbf{z}$ in L dimensions (the union of the yellow and gray areas in Figure 1.3); this is simply the product of its components $\ell \in \mathcal{L}$. Then subtract from $\overline{V}_{\mathbf{z}}$ the volume of G prior to the addition of $\mathbf{z}$ (the union of the gray and white areas in Figure 1.3). The last step is to compute and add back in the volume of the sides of G that were subtracted in the previous step (the white areas in Figure 1.3). This volume is computed by taking the sum over each dimension $\ell \in \mathcal{L}$ of the areas along that dimension enclosed by the existing solutions in G. Pseudocode for the algorithm is presented in Figure 1.4.

Figure 1.3: **Computing the hypervolume of a 3D frontier**. Consider a three-dimensional frontier Z. We sequentially add solutions to a 2D projection of the frontier, seen here (process moves from left to right). The solutions are added in order of decreasing value in their third component (height – not seen here). At each iteration, we compute the contribution in 2D as follows: Add the product of the solution's 2D components (the union of the yellow and gray areas). Then subtract all the previous existing frontier area (the union of the gray and white areas). Then add back the value of the sides (white areas). This yields the value of the yellow area. Multiply this value by the third component of the solution to obtain the solution's contribution to the hypervolume V.
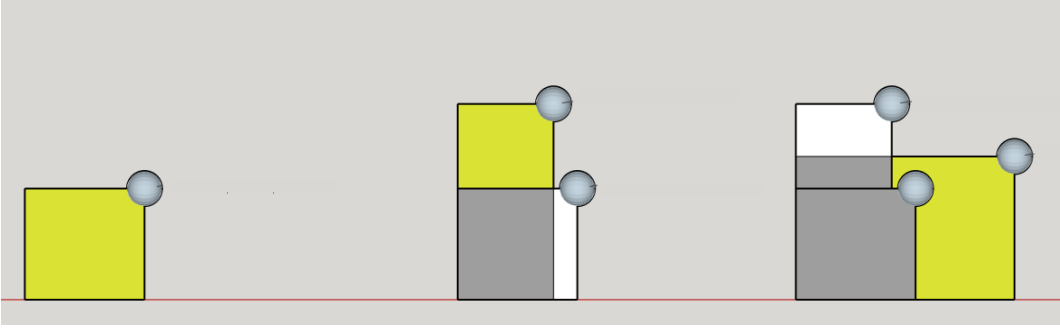
When comparing multi-objective systems, a decision maker may observe unequal hypervolumes across frontiers. Without another means to measure of conflict, the decision maker cannot determine why the inequality exists. Which objective pairs are causing the differences in system-level conflict? We propose here a new conflict metric created specifically to address this question.

1.2.3 A new measure of pairwise conflict

Consider the frontiers in Figure 1.5. The conflict between maximization objectives i and j is greatest in Frontier C and least in Frontier A.

Many authors have previously measured conflict between objectives [10][60][33], with most commonly used metrics deriving from measures of linear correlation (such as the Pearson correlation coefficient [22]) or rank correlation (such as Kendall's Tau [42] or Spearman's rho [44]). The motivation behind these metrics is often the removal of redundant objectives from a many-objective optimization problem. In such cases, measures of monotonicity or correlation alone suffice. However, the current metrics fall short of providing a quantification of conflict between pairs of objectives. Metrics for linear correlation are limited in their ability to capture the montonicity between objectives, which is the fundamental principle that determines if objectives conflict. Furthermore, both linear and rank correlation metrics fail to capture the objective achievement of the solutions. Thus, for a more nuanced understanding of the relationship between the objectives, a different metric is required.

Let $\mathbf{z}_{ij}$ be the sub-dimensional objective vector comprised of only the components corresponding to the ith and jth objectives $\mathbf{z}_{ij} = [z_i, z_j]$. I define the following measure of conflict between objectives i and j:

$$C_{ij} = \frac{(1 - \rho_{ij})\bar{d}_{ij}}{2d_{\max,ij}} \tag{1.17}$$

where $\bar{d}_{ij}$ is the average sub-dimensional distance from objective vectors to the ideal solution:

$$\bar{d}_{ij} = \frac{1}{|Z|} \sum_{\mathbf{z} \in Z} ||\mathbf{z}_{ij}^{\text{ideal}} - \mathbf{z}_{ij}|| \tag{1.18}$$

and

$$d_{\max,ij} = ||\mathbf{z}_{ij}^{\text{ideal}} - \mathbf{z}_{ij}^{\text{nadir}}|| \tag{1.19}$$

and ρ_{ij} is Spearman's rank-correlation coefficient for the solutions' achievements in objectives i and j. Note that $C_{ij} \in [0, 1)$, taking smaller values when there is less conflict between objectives i and j and larger values when there is more.

The conflict metric proposed here (equation (1.17)) addresses two major issues:

1. **Indifference to non-conflicting relationships**. Per equation (1.13), when an objective i increases monotonically with another objective j, the objectives do not conflict. Accordingly, C_{ij} should equal 0 in all such cases. This is true for the new metric, since for monotonically increasing objectives $\rho_{ij} = 1$, so $1 - \rho_{ij} = 0$.

2. **Consideration of objective achievement**. Recall Figure 1.5 and the intuitive notion that the conflict between objectives i and j is stronger in Frontier C than it is in Frontier B than it is in Frontier A. This notion is guided by the idea that the closer objective vectors are to the sub-dimensional ideal solution on average, the less the conflict between the objectives; that is, that greater simultaneous objective provision is indicative of less conflict. The proposed metric accounts for this, while correlation measures do not. In the extreme case of monotonically decreasing objectives, $\frac{(1-\rho_{ij})}{2} = 1$, so $C_{ij} = \frac{\bar{d}ij}{d_{\max,ij}}$. See Figure 1.6 for an example.

1.2.4   Case Study

We demonstrate the novel utility of the existing and proposed conflict metrics on a multi-objective scenario-based case study on forest management in the Deschutes National Forest. In the case study, we seek to minimize fire hazard and sediment delivery while maximizing habitat for the northern spotted owl. We compare conflict and objective achievement under multiple climate change scenarios.

Study system

We study the joint provision of forest ecosystem services under multiple climate change scenarios in the Drink Planning Area, located in the Deschutes National Forest. The Drink Area is a 7056 ha area on the east slopes of the Cascade Mountain Range (see Figure 1.7). Like many forests, the Drink Area is managed for the simultaneous provision of multiple

ecosystem services. For this case study, we selected the maximization of habitat for the northern spotted owl, the minimization of fire hazard, and the minimization of sediment delivery. The Forest Service seeks to ensure the sustained provision of these ecosystem services, which may require an understanding of how these ecosystem services are impacted by climate change.

The first ecosystem service is the provision of habitat for the northern spotted owl (NSO) (*Strix occidentalis caurina*). The NSO is a common, if controversial, indicator species in Pacific Northwest forests. Because of the availability of dense old growth forest in the Drink Area, approximately 43% of the area serves as habitat for the NSO (see Figure 1.8). The USFS is required to protect this species, because it is listed as threatened and therefore protected by the Endangered Species Act of 1973 [13].

The second ecosystem service is protection from high severity wildfire. This protection is achieved by applying silvicultural treatments to designated treatment areas (forest stands) throughout the Drink Area. The types of treatments assigned to stands are defined in the appendix, §B. We measure the fire hazard rating of a stand before and after treatment to assess the treatment's efficacy. The fire hazard rating used here is described in more detail later and is summarized in Table 1.1. The USFS implements silvicultural treatments to reduce the fire hazard rating in order to protect the habitat of the NSO and also to protect the municipal watershed for the cities of Bend, OR and Sisters, OR which lies largely within the boundaries of the Drink Area (see Figure 1.8). Wildfires pose a threat to these cities' water supply, because wildfires can cause soil water repellency, surface runoff, and debris torrents [40] which would degrade the quality of the watershed. In addition, the Drink Area has never before undergone silvicultural treatments, which increases the expected severity of a fire should one occur.

Finally, we seek to minimize sediment delivery into the watershed. While the silvicultural treatments intend to provide long-term protection of the watershed, the disturbance caused by implementing the treatments has the potential to induce short-term increases in sediment delivery [56]. This is expected to be especially true in the Drink Area, where local Forest

Service staff have noted that the watershed is unusually susceptible to spikes in sediment delivery as a result of foot traffic and other activities that occur within the watershed.

These ecosystem services and their relationships with one another will likely be altered by the changing climate. The extent of these changes will depend on the severity of the realized climate change. Thus, to understand the potential impacts, multiple climate change scenarios representing a range of severities must be considered. The following section describes the climate scenarios considered in this case study.

Climate Scenarios Considered

In their assessments on the changing climate, the Intergovernmental Panel on Climate Change (IPCC) uses a scenario-based approach, considering many models of future climates from research groups around the world. They make no attempt to predict which of the future climates is most likely or to quantify the probability of realization of any one scenario. This same scenario-based approach is employed here in studying the potential impacts of climate change on trade-off relationships among bundled ecosystem services. Each scenario considered here results in a distinct multi-objective model and efficient frontier. We choose three climate scenarios for analysis. They were chosen from the set of climate models used by first working group (WG1) in the IPCC's Fifth Assessment (AR5) [39]. The scenarios will henceforth be referred to as "None", "Ensemble RCP 4.5" (or "E45"), and "Ensemble RCP 8.5" (or "E85").

The first scenario, "None", is the assumption of no climate change. While the number of studies incorporating climate change is increasing, this is still the assumption used for many modern studies such as Schroder *et al.* (2013) [65]. Because it has served as the basis for many studies and assumes a static climate resembling today's, the "None" climate scenario serves as a control against which to compare the other two climate scenarios.

As their names suggest, the second and third scenarios are ensembles. Each ensemble is an assembly of 17 global circulation models (GCMs) used in IPCC AR5. The selection of component GCMs in the ensembles was performed by the USFS's Climate-Forest Vegetation

Simulator (FVS) [25] team. The list of the 17 scenarios included in the ensemble can be found in Crookston (2016) [16]. Each component GCM has a corresponding climate surface which contains a vector of 35 climate parameters at over 11,000 global locations for three time periods (2035, 2065, and 2095). The climate surfaces for the ensembles were created by averaging the values of all component GCMs for each climate parameter and each time period for each location. The result is a climate surface that, while temporally sparse, is spatially robust. Such a configuration is well-suited for use in the Drink Area given the area's variance in elevation and slow vegetation growth.

The two ensembles are comprised of the same 17 GCMs, but the assumed representative concentration pathway (RCP) in the component GCMs differ. The RCP indicates the additional radiative forcing in W/m^2 above pre-industrial levels, with higher values of forcing indicative of more severe climate change. The GCMs in the Ensemble RCP 4.5 scenario assume 4.5 W/m^2 of additional radiative forcing, and the GCMs in the Ensemble RCP 8.5 scenario assume 8.5 W/m^2 of additional radiative forcing.

These three chosen scenarios represent a range of predicted climate change severity, from a $0°C$ warming by the year 2100 under the "None" scenario to a $2.6 - 4.8°C$ warming under RCP 8.5 [39]. Using a range of climate change severities should produce efficient frontiers and conflict relationships among the objectives that allow for the demonstration of the comparison methods proposed in sections 1.2.2 and 1.2.3.

1.2.5   The Multi-objective Optimization Model

For each of the three climate scenarios specified in section 1.2.4, we parameterize and solve the following multi-objective zero-one mathematical program that optimizes the joint provision of ecosystem services in the Drink Area. The model operates over an 80-year planning horizon (2015-2095). In the planning horizon, there are two treatment periods (2015-2035 and 2035-2055). The model decides on which stands and in which periods to perform silvicultural treatments. Determining the treatment to apply to a stand was done *a priori* and is dependent only on silvicultural characteristics at the time of treatment; the rules governing

the assignment of treatment types can be found in the appendix, §B.

The model minimizes the fire hazard rating of the Drink Area at the end of the 80-year planning horizon, maximizes the area of NSO habitat at the end of each planning period, and minimizes the short-term spikes in sediment delivery resulting from the application of silvicultural treatments. Treatments are assumed to be performed at the midpoint year in the treatment periods: years 2025 and 2045 for the first and second periods, respectively. Figure 1.9 contains a schematic of the planning horizon showing the time of these events.

Notation

The following notation is used throughout the model:

Parameters

- $i \in I$: the set of forest stands comprising the Drink Area ($|I| = 303$)

- $r \in R$: the set of treatment schedule prescriptions:

$$r = \begin{cases} 1 & \text{treatment applied in the first period (2015-2035)} \\ 2 & \text{treatment applied in the second period (2035-2055)} \\ 3 & \text{treatment applied in both periods} \\ 0 & \text{no treatment applied in either period} \end{cases}$$

- $F_{i,r}$: the area-weighted fire hazard rating of stand i at the end of the planning horizon if prescribed to treatment schedule r

- $I_{\omega,t}$: the set of stands that qualify as NSO habitat at the end of planning period t under at least one treatment schedule

- a_i: the area of stand i

- e: the discount factor applied to NSO habitat when it is not part of a contiguous habitat cluster at least 200 ha in size

- $j \in R_{i,t}$: the set of treatment schedules such that stand i qualifies as NSO habitat in planning period t

- $s_{i,t}$: the amount of sediment (in tons) delivered to the watershed as a result of performing fuel treatments on stand i in planning period t

- $c \in C$: the set of all clusters of stands whose combined area exceeds 200 hectares

- $i \in D_c$: the set of all stands that comprise cluster c

- $c \in C_i$: the set of all clusters that contain stand i

- A: the maximum area in hectares that may be treated in either planning period

- ℓ, u: the lower and upper bounds, respectively, on the relative fluctuation in the area treated in periods 1 and 2

Decision Variables

$$
x_{i,r} = \begin{cases} 1 & \text{if stand } i \text{ is prescribed to treatment schedule } r \\ 0 & \text{otherwise} \end{cases}
$$

Indicator Variables

- $q_{c,t} = 1$ if all stands in cluster c qualify as NSO habitat at the end of planning period t; $q_{c,t} = 0$ otherwise

- $p_{i,t} = 1$ if in planning period t stand i is part of a cluster c such that $q_{c,t} = 1$; $p_{i,t} = 0$ otherwise

Accounting Variables

- S_t: the total sediment delivered to the watershed from performing fuel treatments in planning period t

- O_t: the amount of NSO habitat (in hectares) at the end of planning period t

- H_t: the total area (in hectares) treated in planning period t

Parameterization

The model was parameterized as follows:

- $F_{i,r}$: the metric for fire hazard rating used in this analysis originated in the work by Schroder *et al.* [65]. This metric was developed for the Drink Area. It uses fire characteristics from Anderson's fuel models [4] to assign a fire hazard rating. I expanded the rating system to include fuel models not present in Schroder *et al.* See Table 1.1.

  The stands' fuels and vegetation characteristics to determine the fire hazard rating were generated using the US Forest Service's Climate-Forest Vegetation Simulator (Climate-FVS). Input vegetation data to Climate-FVS came from the 2012 GNN structure map (http://lemma.forestry.oregonstate.edu/data/structure-maps) from Oregon State University's Landscape Ecology, Modeling, Mapping & Analysis (LEMMA) group. Plots from the LEMMA database were mapped to the stands in the Drink area in order to produce tree and stand lists. These lists were used with Climate-FVS to simulate the stands' vegetation and fuels characteristics forward for the duration of the planning horizon under each climate scenario. Input climate data for Climate-FVS was obtained through the Climate-FVS climate data server [17].

- $I_{\omega,t}$: the set of stands that qualify as NSO habitat at the end of a planning period t are those that meet the following three criteria, as specified by the USFS:

1. elevation less than 1830 m

2. the presence of trees with diameter at breast height (DBH) at least than 76 cm

3. canopy closure of at least 60%

The elevation requirement was checked using a digital elevation model from the US Department of Agriculture's GeoSpatial Data Gateway; canopy closure and large tree criteria were determined using the simulated vegetation characteristics output from Climate-FVS.

To account for the NSO's large habitat requirements, stands must also be members of a cluster exceeding 200 ha in size, the entirety of which meets the aforementioned NSO habitat criteria. Stands that meet the first three criteria but are not part of such a cluster have their contributions to the total owl habitat discounted by a factor of e.

- e: the discount factor for sub-200 ha NSO habitat was set to $e = 0.5$ following the convention used in Schroder *et al.* [65].

- $j \in R_{i,t}$: each combination of stand-treatment schedule is evaluated at the end of each planning period to determine its suitability as NSO habitat. The set $R_{i,t}$ consists of treatment schedules for which stand i meets the NSO habitat criteria at the end of treatment period t.

- $s_{i,t}$: the contributions of sediment delivery from treatment of stand i in period t were determined using the Watershed Erosion Prediction Project (WEPP) online GIS tool [31]. This tool takes as input soil textures, treatment types, duration of simulation, and custom climate data. Soil texture data for the Drink area was obtained from the USDA's Soil Survey Geographic (SSURGO) database, treatment types are those specified in §B, and the years of simulation correspond to the treatment years in the model's planning horizon (2015-2095). The custom climate data are those described above for use with Climate-FVS, obtained through the Climate-FVS data server.

- C,D_c,C_i: the formulation of clusters was performed *a priori* according to the algorithm used in Rebain and McDill (2003) [61]. The enumerated clusters can then be used to immediately determine cluster members D_c and stand-owning clusters C_i.

- A: the maximum area that may be treated in either planning period was defined to be 6000 acres, or approximately 2428 ha

- ℓ, u: the relative fluctuation in the area treated in periods 1 and 2 was defined to be 20%. That is, the lower bound $\ell = 0.8$, and the upper bound $u = 1.2$.

Fuel Model	Fire Hazard Rating	Group	Flame length (m)	Rate of spread (m/hr)	Total fuel load (tons/ha)
4*	5	Shrub	5.79	1508.76	32.12
5	4	Shrub	1.22	362.10	8.65
8	1	Timber	0.30	32.19	12.36
9*	2	Timber	0.79	150.88	8.65
10	2	Timber	1.46	158.92	29.65
11*	2	Logging Slash	1.07	120.7	28.42
12	4	Logging Slash	2.44	261.52	85.50
13	5	Logging Slash	3.20	271.58	143.57

Table 1.1: Fire hazard rating system used here, originally employed by Schroder *et al.* [65]. Asterisks (*) denote fuel models not present in Schroder *et al.*
The fuel model column refers to the Anderson fuel model ratings [4].

Formulation

The formulation of the multi-objective model is as follows:

$$Minimize$$

$$\sum_{i \in I} \sum_{r \in R} F_{i,r} x_{i,r} \tag{1.20}$$

$$\max\{S_1, S_2\} \tag{1.21}$$

$$Maximize$$

$$\min\{O_1, O_2\} \tag{1.22}$$

Subject to:

$$\sum_{i\in I_{\omega,t}}\left(a_i p_{i,t} + ea_i\left(\sum_{j\in R_{i,t}} x_{i,j} - p_{i,t}\right)\right) = O_t \qquad \forall t \in \{1,2\} \qquad (1.23)$$

$$\sum_{i\in I}\sum_{r\in 1,3} s_{i,1} x_{i,r} = S_1 \qquad (1.24)$$

$$\sum_{i\in I}\sum_{r\in 2,3} s_{i,2} x_{i,r} = S_2 \qquad (1.25)$$

$$\sum_{i\in D_c}\sum_{j\in R_{i,t}} x_{i,j} - |c| q_{c,t} \geq 0 \qquad \forall t \in \{1,2\}, c \in C \qquad (1.26)$$

$$\sum_{c\in C_i} q_{c,t} - p_{i,t} \geq 0 \qquad \forall t \in \{1,2\}, i \in I_{\omega,t} \qquad (1.27)$$

$$\sum_{r\in R} x_{i,r} = 1 \qquad \forall i \in I \qquad (1.28)$$

$$\sum_{i\in I}\sum_{r\in 1,3} a_i x_{i,r} = H_1 \qquad (1.29)$$

$$\sum_{i\in I}\sum_{r\in 2,3} a_i x_{i,r} = H_2 \qquad (1.30)$$

$$H_t \leq A \qquad \forall t \in \{1,2\} \qquad (1.31)$$

$$\ell H_1 - H_2 \leq 0 \qquad (1.32)$$

$$-u H_1 + H_2 \leq 0 \qquad (1.33)$$

$$x_{i,r}, p_i, q_c \in \{0,1\} \quad \forall i \in I, r \in R, c \in C \qquad (1.34)$$

Equations (1.20)-(1.22) are the objective functions: equation (1.20) minimizes the cumulative fire hazard rating of the Drink Area at the end of the 80-year planning horizon, equation (1.21) minimizes the maximum peak in sediment delivery for the two planning periods, and equation (1.22) maximizes the minimum NSO habitat available at the end of the planning periods. Equation set (1.23) defines the amount of NSO habitat available at the end of the planning horizons. Note that if stand i does not belong to a cluster of NSO habitat exceeding 200 hectares, then its area contribution to total NSO habitat is discounted by a factor of e. Equations (1.24) and (1.25) define the sediment delivered in planning periods

one and two, respectively.

Inequality set (1.26) controls the value of the cluster variables $q_{c,t}$ indicating clusters meeting NSO habitat criteria in each of the planning periods. Inequality set (1.27) controls the value of the $p_{i,t}$ variables indicating stands' inclusion in NSO habitat clusters.

The set of equalities (1.28) enforces the logical constraint that each stand must be prescribed to exactly one treatment schedule. Equations (1.29) and (1.30) are accounting constraints for the total area treated in each planning period, and inequalities (1.31) ensure that this area does not exceed the predefined per-period maximum. Inequalities (1.32) and (1.33) bound the fluctuation in treated area between the planning periods. Finally, constraint (1.34) defines the decision and indicator variables as binary.

Solution method

I developed an implementation of Tóth's Alpha-Delta algorithm [72] to solve the model for each climate change scenario utilizing the IBM ILOG CPLEX optimization engine. For a problem with M objectives, the Alpha-Delta algorithm finds the optimal set of solutions by iteratively slicing the M-dimensional objective space with a tilted $M - 1$-dimensional hyperplane. The algorithm was implemented using an alpha parameter of $\alpha = .01$ and delta parameters of $\delta_{Hab} = 1$ ha and $\delta_{Sed} = 2$ tons for the NSO habitat and sediment delivery objectives, respectively.

1.3 Results and Discussion

We first provide the results of the case study, and then we give more general results about the application of conflict-measuring methods to multiple multi-objective systems.

1.3.1 Case Study Results

We parameterized and solved the multi-objective model ((1.20)-(1.34)) for each of the climate scenarios, generating three efficient frontiers: Z_{None}, $Z_{4.5}$, and $Z_{8.5}$ for the None, Ensemble

RCP 4.5, and Ensemble RCP 8.5 scenarios, respectively. Summary details for each frontier are shown in Table MAKETABLE, and the frontiers are shown in Figure MAKEFIGURE.

1.4 Conclusion

DRAFT

I find that climate change has positive impacts on the tradeoff structure between managed ecosystem services in the Drink Area ...

Figure 1.4: Algorithm to compute the hypervolume V of a Pareto frontier. Prior to running the algorithm, pick an objective m from the objective set $\mathcal{M}$ and define the sub-dimensional objective set $\mathcal{L} = \mathcal{M} \backslash \{m\}$. Then sort $\mathbf{z} \in Z$ in descending order by their mth component. Here, $\mathbf{z} \in Z$ is the set of relative objective vectors. Let $\overline{V_{\mathbf{z}}}$ be the $(M-1)$-dimensional volume contribution of the solution $\mathbf{z}$, and let $\mathbf{g} \in G$ be the non-dominated objective vectors in $M-1$ dimensions.

1:   $V \leftarrow 0$

2:   $\overline{V} \leftarrow 0$

3:   $G \leftarrow \emptyset$

4:   **for all** $\mathbf{z} \in Z$ **do**

5:      $\overline{V}_{\mathbf{z}} \leftarrow \prod_{\ell \in \mathcal{L}} z_\ell - \overline{V}$

6:      **for all** $\mathbf{g} \in G$ **do**

7:        **if** $g_\ell < z_\ell \, \forall \ell \in \mathcal{L}$ **then**

8:          $G \leftarrow G \backslash \{\mathbf{g}\}$

9:        **end if**

10:      **end for**

11:      **for all** $\ell \in \mathcal{L}$ **do**

12:        $G_{\mathbf{z},\ell} := \{\, \mathbf{g} \in G : g_\ell > z_\ell \,\}$

13:        Sort $\mathbf{g} \in G_{\mathbf{z},\ell}$ in ascending order by ℓth component, g_ℓ

14:        $v_i \leftarrow z_\ell$

15:        **for all** $\mathbf{g} \in G_{\mathbf{z},\ell}$ **do**

16:          $v_t \leftarrow g_\ell$

17:          $\delta_\ell := v_t - v_i$

18:          $\overline{V}_{\mathbf{z}} \leftarrow \overline{V}_{\mathbf{z}} + \delta_\ell \prod_{\lambda \in \mathcal{L} \backslash \{\ell\}} g_\lambda$

19:          $v_i \leftarrow v_t$

20:        **end for**

21:      **end for**

22:      $G \leftarrow G \cup \{\mathbf{z}\}$

23:      $\overline{V} \leftarrow \overline{V} + \overline{V}_{\mathbf{z}}$

24:      $V \leftarrow V + z_m \overline{V}_{\mathbf{z}}$
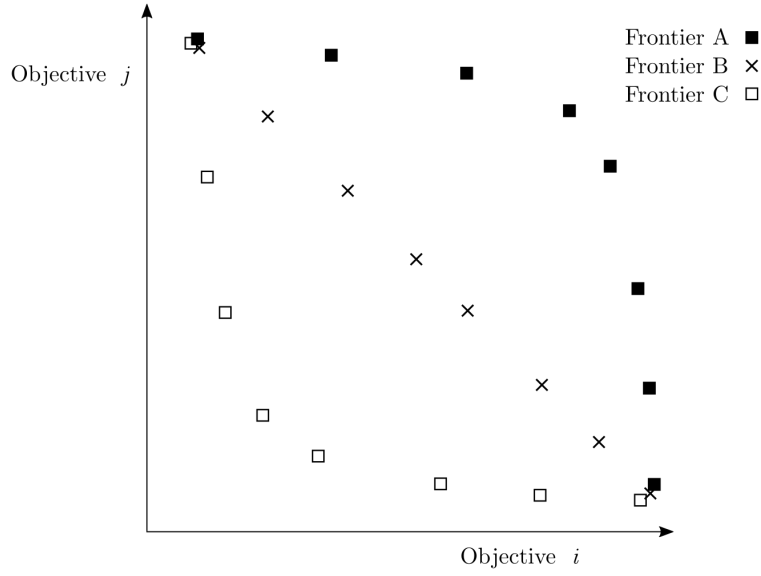
25: **end for**

Figure 1.5: Varying conflict between objectives. The conflict between maximization objectives i and j increases from Frontier A to Frontier B to Frontier C.

	Proposed C_{ij}	Pearson ρ_{ij}	Spearman $\rho_{s,ij}$
Frontier A	0.4	-0.6	-1
Frontier B	0.6	-1	-1
Frontier C	0.8	-0.6	-1

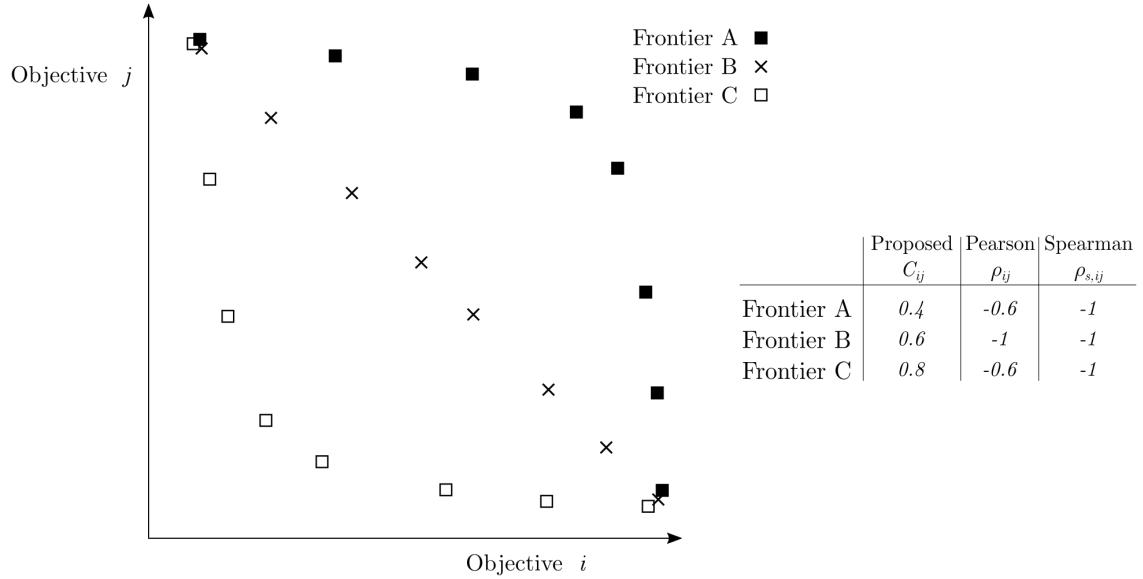Figure 1.6: Comparing the proposed metric for conflict C_{ij} against the Pearson product-moment and the Spearman rank correlation coefficients (ρ_{ij} and $\rho_{s,ij}$, respectively). While the latter two are identical for frontiers A and C, the proposed metric is greater for frontier C than it is for A. This is because it accounts for the average relative distance to the sub-dimensional ideal objective vector.

Figure 1.7: Overview of the study system, the Drink Planning Area (in purple), consisting of 7056 ha in the Deschutes National Forest.
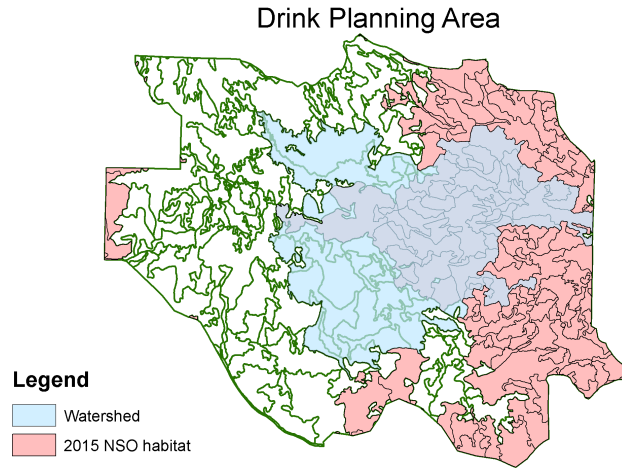
Figure 1.8: Location of the municipal watershed and the suitable NSO habitat in the Drink area at the beginning of the planning horizon (2015). Interior polygons are the 303 management units.
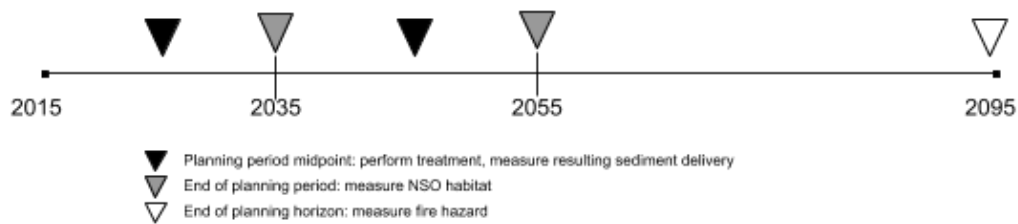
Figure 1.9: The planning horizon used in the case study spans the 80 year period from 2015 to 2095. Treatments may be performed in the first period, the second period, both, or neither. Treatments are assumed to be performed at the mid-point years of each period (black triangles). Sediment delivery is measured on treatment years. Stands' suitability for NSO habitat is measured at the end of the planning periods (gray triangles), and stands' fire hazard ratings are measured at the end of the planning horizon (white triangle).

BIBLIOGRAPHY

[1] 36 CFR 219.1. National forest system land management planning, 2012.

[2] Fouad Ben Abdelaziz. Solution approaches for the multiobjective stochastic programming. *European Journal of Operational Research*, 216(1):1–16, 2012.

[3] Frank A Albini. Estimating wildfire behavior and effects. 1976.

[4] Hal E Anderson. Aids to determining fuel models for estimating fire behavior. *The Bark Beetles, Fuels, and Fire Bibliography*, page 143, 1982.

[5] Millennium Ecosystem Assessment et al. *Ecosystems and human well-being*, volume 5. Island press Washington, DC:, 2005.

[6] Brad Bass, Guohe Huang, and Joe Russo. Incorporating climate change into risk assessment using grey mathematical programming. *Journal of Environmental Management*, 49(1):107 – 123, 1997.

[7] Gordon B Bonan. Forests and climate change: forcings, feedbacks, and the climate benefits of forests. *Science*, 320(5882):1444–1449, 2008.

[8] Jose G Borges, Jordi Garcia-Gonzalo, Vladimir Bushenkov, Marc E McDill, Susete Marques, and Manuela M Oliveira. Addressing multicriteria forest management with pareto frontier methods: An application in portugal. *Forest Science*, 60(1):63–72, 2014.

[9] Dimo Brockhoff and Eckart Zitzler. Are all objectives necessary? on dimensionality reduction in evolutionary multiobjective optimization. In *Parallel Problem Solving from Nature-PPSN IX*, pages 533–542. Springer, 2006.

[10] Dimo Brockhoff and Eckart Zitzler. Objective reduction in evolutionary multiobjective optimization: Theory and applications. *Evolutionary Computation*, 17(2):135–166, 2009.

[11] Brett A. Bryan and Neville D. Crossman. Systematic regional planning for multiple objective natural resource management. *Journal of Environmental Management*, 88(4):1175 – 1189, 2008.

[12] Kai MA Chan, M Rebecca Shaw, David R Cameron, Emma C Underwood, and Gretchen C Daily. Conservation planning for ecosystem services. *PLoS biology*, 4(11):e379, 2006.

[13] US Congress. Endangered species act. *Washington DC*, 1973.

[14] Ira R. Cooke, Simon A. Queenborough, Elizabeth H. A. Mattison, Alison P. Bailey, Daniel L. Sandars, A. R. Graves, J. Morris, Philip W. Atkinson, Paul Trawick, Robert P. Freckleton, Andrew R. Watkinson, and William J. Sutherland. Integrating socio-economics and ecology: a taxonomy of quantitative methods and a review of their use in agro-ecology. *Journal of Applied Ecology*, 46(2):269–277, 2009.

[15] Steven P Courtney and Andrew B Carey. *Scientific evaluation of the status of the Northern Spotted Owl*. Sustainable Ecosystems Institute Portland, OR, 2004.

[16] Nicholas Crookston. Details of data and methods used for calculating future climate estimates, 2016.

[17] Nicholas Crookston. Get climate-fvs ready data, 2016.

[18] Nicholas L Crookston. Climate-fvs version 2: Content, users guide, applications, and behavior. 2014.

[19] Piotr Czyzżak and Adrezej Jaszkiewicz. Pareto simulated annealingâĂŤa metaheuristic technique for multiple-objective combinatorial optimization. *Journal of Multi-Criteria Decision Analysis*, 7(1):34–47, 1998.

[20] Gretchen C Daily, Susan Alexander, Paul R Ehrlich, Larry Goulder, Jane Lubchenco, Pamela A Matson, Harold A Mooney, Sandra Postel, Stephen H Schneider, David Tilman, et al. *Ecosystem services: benefits supplied to human societies by natural ecosystems*, volume 2. Ecological Society of America Washington (DC), 1997.

[21] Kalyanmoy Deb. *Multi-objective optimization using evolutionary algorithms*, volume 16. John Wiley & Sons, 2001.

[22] Kalyanmoy Deb and D Saxena. Searching for pareto-optimal solutions through dimensionality reduction for certain large-dimensional multi-objective optimization problems. In *Proceedings of the World Congress on Computational Intelligence (WCCI-2006)*, pages 3352–3360, 2006.

[23] Kalyanmoy Deb and Dhish Kumar Saxena. On finding pareto-optimal solutions through dimensionality reduction for certain large-dimensional multi-objective optimization problems. *Kangal report*, 2005011, 2005.

[24] Luis Diaz-Balteiro and Carlos Romero. Making forestry decisions with multiple criteria: a review and an assessment. *Forest Ecology and Management*, 255(8):3222–3241, 2008.

[25] Gary E Dixon et al. Essential fvs: A userâĂŹs guide to the forest vegetation simulator. *Fort Collins, CO: USDA-Forest Service, Forest Management Service Center*, 2002.

[26] German Climate Computing Centre (DKRZ). IPCC working group i AR5 snapshot.

[27] Oregon Fish and Wildlife Office. Species fact sheet: Northern spotted owl. `http://www.fws.gov/oregonfwo/Species/Data/NorthernSpottedOwl/default.asp`. Accessed: 2015-02-06.

[28] US Fish, Wildlife Service, et al. Revised recovery plan for the northern spotted owl (strix occidentalis caurina). *USDI Fish and Wildlife Service, Portland, OR USA*, 2011.

[29] Forestières Internationaler Verband Forstlicher Forschungsanstalten. Adaptation of forests and people to climate change. 2009.

[30] Eclipse Foundation. Eclipse, 2014.

[31] James R Frankenberger, Shuhui Dun, Dennis C Flanagan, Joan Q Wu, and William J Elliot. Development of a gis interface for WEPP model application to great lakes forested watersheds. In *International Symposium on Erosion and Landscape Evolution (ISELE), 18-21 September 2011, Anchorage, Alaska*, page 139. American Society of Agricultural and Biological Engineers, 2011.

[32] William L Gaines, Richy J Harrod, James Dickinson, Andrea L Lyons, and Karl Halupka. Integration of northern spotted owl habitat and fuels treatments in the eastern cascades, washington, usa. *Forest Ecology and Management*, 260(11):2045–2052, 2010.

[33] Tomas Gal and Heiner Leberling. Redundant objective functions in linear vector maximum problems and their determination. *European Journal of Operational Research*, 1(3):176–184, 1977.

[34] J Garcia-Gonzalo, JG Borges, JHN Palma, and A Zubizarreta-Gerendiain. A decision support system for management planning of eucalyptus plantations facing climate change. *Annals of Forest Science*, 71(2):187–199, 2014.

[35] Jaime R. Goode, Charles H. Luce, and John M. Buffington. Enhanced sediment delivery in a changing climate in semi-arid mountain basins: Implications for water resource management and aquatic habitat in the northern rocky mountains. *Geomorphology*, 139âĂŞ140(0):1 – 15, 2012.

[36] Lee E Harding and Emily McCullum. Ecosystem response to climate change in british columbia and yukon: threats and opportunities for biodiversity. *Responding to global climate change in British Columbia and Yukon*, 1:9–1, 1997.

[37] Grant Hauer, Steve Cumming, Fiona Schmiegelow, Wiktor Adamowicz, Marian Weber, and Robert Jagodzinski. Tradeoffs between forestry resource and conservation values under alternate policy regimes: A spatial analysis of the western canadian boreal plains. *Ecological Modelling*, 221(21):2590 – 2603, 2010.

[38] Anke K Hutzschenreuter, Peter AN Bosman, and Han La PoutrÚ. Evolutionary multiobjective optimization for dynamic hospital resource management. In *International Conference on Evolutionary Multi-Criterion Optimization*, pages 320–334. Springer, 2009.

[39] IPCC Working Group I. *Climate Change 2013-The Physical Science Basis: Summary for Policymakers*. Intergovernmental Panel on Climate Change, 2013.

[40] George G Ice, Daniel G Neary, and Paul W Adams. Effects of wildfire on soils and watershed processes. *Journal of Forestry*, 102(6):16–20, 2004.

[41] Louis R Iverson and Anantha M Prasad. Predicting abundance of 80 tree species following climate change in the eastern united states. *Ecological Monographs*, 68(4):465–485, 1998.

[42] Evangelos Kanoulas and Javed A Aslam. Empirical justification of the gain and discount function for ndcg. In *Proceedings of the 18th ACM conference on Information and knowledge management*, pages 611–620. ACM, 2009.

[43] Amit Kanudia and Richard Loulou. Robust responses to climate change via stochastic markal: The case of quÃľbec. *European Journal of Operational Research*, 106(1):15 – 30, 1998.

[44] Prasad Karande and Shankar Chakraborty. Application of multi-objective optimization on the basis of ratio analysis (moora) method for materials selection. *Materials & Design*, 37:317–324, 2012.

[45] Vineet Khare, Xin Yao, and Kalyanmoy Deb. Performance scaling of multi-objective evolutionary algorithms. In *Evolutionary Multi-Criterion Optimization*, pages 376–390. Springer, 2003.

[46] Joshua Knowles and David Corne. On metrics for comparing nondominated sets. In *Evolutionary Computation, 2002. CEC'02. Proceedings of the 2002 Congress on*, volume 1, pages 711–716. IEEE, 2002.

[47] Danny C Lee and Larry L Irwin. Assessing risks to spotted owls from forest thinning in fire-adapted forests of the western united states. *Forest Ecology and Management*, 211(1):191–209, 2005.

[48] Marcus Linder. Developing adaptive forest management strategies to cope with climate change. *Tree Physiology*, 20(5-6):299–307, 2000.

[49] Alexander V Lotov, Vladimir A Bushenkov, and Georgy K Kamenev. *Interactive decision maps: Approximation and visualization of Pareto frontier*, volume 89. Springer, 2004.

[50] Alexander V Lotov and Kaisa Miettinen. Visualizing the pareto frontier. In *Multiobjective optimization*, pages 213–243. Springer, 2008.

[51] B Luo, I Maqsood, YY Yin, GH Huang, and SJ Cohen. Adaption to climate change through water trading under uncertainty- an inexact two-stage nonlinear programming approach. *Journal of Environmental Informatics*, 2(2):58–68, 2003.

[52] Shunsuke Managi. Evaluation and policy analysis of japanese forestry. In *2005 Annual meeting, July 24-27, Providence, RI*, number 19358. American Agricultural Economics Association (New Name 2008: Agricultural and Applied Economics Association), 2005.

[53] Donald McKenzie, Ze'ev Gedalof, David L Peterson, and Philip Mote. Climatic change, wildfire, and conservation. *Conservation Biology*, 18(4):890–902, 2004.

[54] Robin Naidoo, Andrew Balmford, Robert Costanza, Brendan Fisher, Rhys E Green, B Lehner, TR Malcolm, and Taylor H Ricketts. Global mapping of ecosystem services and conservation priorities. *Proceedings of the National Academy of Sciences*, 105(28):9495–9500, 2008.

[55] Craig R. Nitschke and John L. Innes. Integrating climate change into forest management in south-central british columbia: An assessment of landscape vulnerability and development of a climate-smart framework. 2008.

[56] Jay OâĂŹLaughlin. Conceptual model for comparative ecological risk assessment of wildfire effects on fish, with and without hazardous fuel treatment. *Forest Ecology and Management*, 211(1):59–72, 2005.

[57] Intergovernmental Panel on Climate Change. Definition of terms used within the DDC pages. `http://www.ipcc-data.org/guidelines/pages/definitions.html`, 2013.

[58] Intergovernmental Panel on Climate Change. Scenario Process for AR5. `http://sedac.ipcc-data.org/ddc/ar5\_scenario\_process/scenario\_background.html`, 2014.

[59] M. Pasalodos-Tato, A. MÃďkinen, J. Garcia-Gonzalo, J.G. Borges, T. LÃďmÃěs, and L.O. Eriksson. Review. assessing uncertainty and risk in forest planning and decision support systems: review of classical methods and introduction of new approaches. *Forest Systems*, 22(2), 2013.

[60] Robin C Purshouse and Peter J Fleming. Conflict, harmony, and independence: Relationships in evolutionary multi-criterion optimisation. In *International Conference on Evolutionary Multi-Criterion Optimization*, pages 16–30. Springer, 2003.

[61] Stephanie Rebain and Marc E McDill. A mixed-integer formulation of the minimum patch size problem. *Forest Science*, 49(4):608–618, 2003.

[62] Lester Henry Reineke. Perfecting a stand-density index for even-aged forests. 1933.

[63] Elizabeth Reinhardt and Nicholas L Crookston. The fire and fuels extension to the forest vegetation simulator. 2003.

[64] Jason R Schott. Fault tolerant design using single and multicriteria genetic algorithm optimization. Technical report, DTIC Document, 1995.

[65] Svetlana A (Kushch) Schroder, Sándor F Tóth, Robert L Deal, and Ettl Gregory J. Multi-objective optimization to evaluate tradeoffs among forest ecosystem services following fire hazard reduction in the Deschutes National Forest, USA. *Ecosystem Services*, Special Issue "Integrated Valuation of Ecosystem Services: Challenges and Solutions", accepted.

[66] Svetlana Kushch Schroder. *Optimizing forest management in consideration of environmental regulations, economic constraints, and ecosystem services*. PhD thesis, 2013.

[67] Rupert Seidl, Werner Rammer, Dietmar Jäger, and Manfred J Lexer. Impact of bark beetle (< i> ips typographus</i> l.) disturbance on timber production and carbon sequestration in different management strategies under climate change. *Forest Ecology and Management*, 256(3):209–220, 2008.

[68] José Oscar H Sendín, Antonio A Alonso, and Julio R Banga. Efficient and robust multi-objective optimization of food processing: A novel approach with application to thermal sterilization. *Journal of Food Engineering*, 98(3):317–324, 2010.

[69] Daniel Simberloff. Flagships, umbrellas, and keystones: is single-species management passé in the landscape era? *Biological conservation*, 83(3):247–257, 1998.

[70] Soil Survey Staff. Soil survey geographic (ssurgo) database.

[71] Chris D Thomas, Alison Cameron, Rhys E Green, Michel Bakkenes, Linda J Beaumont, Yvonne C Collingham, Barend FN Erasmus, Marinez Ferreira De Siqueira, Alan Grainger, Lee Hannah, et al. Extinction risk from climate change. *Nature*, 427(6970):145–148, 2004.

[72] Sándor Tóth. *Modeling Timber and Non-timber Trade-offs in Spatially-Explicit Forest Planning*. PhD thesis.

[73] Sándor Tóth and Marc McDill. Finding efficient harvest schedules under three conflicting objectives. 2009.

[74] Sándor Tóth, Marc McDill, and Stephanie Rebain. Finding the efficient frontier of a bi-criteria, spatially explicit, harvest scheduling problem. 2006.

[75] Sándor F Tóth, Gregory J Ettl, Nóra Könnyű, Sergey S Rabotyagov, Luke W Rogers, and Jeffrey M Comnick. Ecosel: multi-objective optimization to sell forest ecosystem services. *Forest Policy and Economics*, 35:73–82, 2013.

[76] Sándor F Tóth and Marc E McDill. Finding efficient harvest schedules under three conflicting objectives. *Forest Science*, 55(2):117–131, 2009.

[77] Fernando Badilla Veliz, Jean-Paul Watson, Andres Weintraub, Roger J-B Wets, and David L Woodruff. Stochastic optimization models in forest planning: a progressive hedging solution approach. *Annals of Operations Research*, pages 1–16, 2014.

[78] James M Vose, David Lawrence Peterson, Toral Patel-Weynand, et al. *Effects of climatic variability and change on forest ecosystems: a comprehensive science synthesis for the US forest sector*. US Department of Agriculture, Forest Service, Pacific Northwest Research Station Portland, OR, 2012.

[79] Yu Wang, Hailian Yin, Shuai Zhang, and Xiongqing Yu. Multi-objective optimization of aircraft design for emission and cost reductions. *Chinese Journal of Aeronautics*, 27(1):52–58, 2014.

[80] Andy White and Alejandra Martin. Who owns the worldâĂŹs forests. *Forest Trends, Washington, DC*, 2002.

[81] Steven M Wondzell and John G King. Postfire erosional processes in the pacific north-west and rocky mountain regions. *Forest Ecology and Management*, 178(1):75–87, 2003.

[82] Rasoul Yousefpour, Jette Bredahl Jacobsen, Bo Jellesmark Thorsen, Henrik Meilby, Marc Hanewinkel, and Karoline Oehler. A review of decision-making approaches to handle uncertainty and risk in adaptive forest management under climate change. *Annals of forest science*, 69(1):1–15, 2012.

[83] Eckart Zitzler. *Evolutionary algorithms for multiobjective optimization: Methods and applications*, volume 63. Citeseer, 1999.

[84] Eckart Zitzler, Lothar Thiele, Marco Laumanns, Carlos M Fonseca, and Viviane Grunert Da Fonseca. Performance assessment of multiobjective optimizers: an analysis and review. *Evolutionary Computation, IEEE Transactions on*, 7(2):117–132, 2003.

Appendix A

COMPUTING A FRONTIER'S HYPERVOLUME INDICATOR

Given an efficient frontier Z comprised of objective vectors $\mathbf{z} = [z_1, \ldots, z_M] \in Z$, this algorithm computes the volume V of the objective space bounded by Z. This value is known as the hypervolume indicator. For more details on the hypervolume indicator, see §C.

The objectives are assumed to be normalized so that the objective space is the M-dimensional unit hypercube with the origin and the point $\vec{\mathbf{1}}$ defining the nadir objective vector and the ideal objective vector, respectively. That is, all objectives are assumed to be maximized and such that

$$\forall i \in \{1, \ldots, M\} \quad z_i \in [0, 1].$$

The algorithm projects the objective space into $M - 1$ dimensions by eliminating the dimension associated with an objective $m \in \mathcal{M}$. We define the sub-dimensional objective set $\mathcal{L} = \mathcal{M} \backslash \{m\}$. It is assumed that $\mathbf{z} \in Z$ are sorted in descending order according to their mth component. The algorithm proceeds by sequentially adding solutions to the $(M - 1)$-dimensional space, and calculating the contribution to the frontier volume V as a product of the volume contribution in $M - 1$ dimensions and z_m.

Let $\overline{V_{\mathbf{z}}}$ be the $(M - 1)$-dimensional volume contribution of solution $\mathbf{z}$. Further, let $\mathbf{f} \in F$ be the non-dominated objective vectors in $M - 1$ dimensions. Compute the hypervolume V as follows:

Figure A.1: Algorithm to compute the unary hypervolume indicator of a Pareto frontier.

1: $V \leftarrow 0$

2: $\overline{V} \leftarrow 0$

3: $F \leftarrow \emptyset$

4: **for all** $\mathbf{z} \in Z$ **do**

5:      $\overline{V}_{\mathbf{z}} \leftarrow \prod_{\ell \in \mathcal{L}} z_\ell - \overline{V}$

6:      **for all** $\mathbf{f} \in F$ **do**

7:          **if** $f_\ell < z_\ell \; \forall \ell \in \mathcal{L}$ **then**

8:              $F \leftarrow F \backslash \{\mathbf{f}\}$

9:          **end if**

10:      **end for**

11:      **for all** $\ell \in \mathcal{L}$ **do**

12:          $F_{\mathbf{z},\ell} := \{ \mathbf{f} \in F : f_\ell > z_\ell \}$

13:          Sort $\mathbf{f} \in F_{\mathbf{z},\ell}$ in ascending order by ℓth component, f_ℓ

14:          $v_i \leftarrow z_\ell$

15:          **for all** $\mathbf{f} \in F_{\mathbf{z},\ell}$ **do**

16:              $v_t \leftarrow f_\ell$

17:              $\delta_\ell := v_t - v_i$

18:              $\overline{V}_{\mathbf{z}} \leftarrow \overline{V}_{\mathbf{z}} + \delta_\ell \prod_{\lambda \in \mathcal{L} \backslash \{\ell\}} f_\lambda$

19:              $v_i \leftarrow v_t$

20:          **end for**

21:      **end for**

22:      $F \leftarrow F \cup \{\mathbf{z}\}$

23:      $\overline{V} \leftarrow \overline{V} + \overline{V}_{\mathbf{z}}$

24:      $V \leftarrow V + z_m \overline{V}_{\mathbf{z}}$

25: **end for**

Appendix B

TREATMENT SPECIFICATIONS FOR THE DRINK AREA

Table B.1 provides a mapping from a stand's vegetation conditions to the treatment action to apply to the stand. If a stand's conditions do not correspond to any row in the table, then no action is taken. The table was adapted from Schroder [65]. The plant association groups in the Drink area are shown in Figure B.1.

Table B.1: Rules governing treatment assignments.

SDI[1]	CBD[2]	TPH$_{<18}$[3]	Fuel model[4]	BA$_{\mathrm{MHD+WF},>46}$[5]	Treatment
Lodgepole pine (LPD) plant association					
< 87	N/A	N/A	N/A	N/A	Prescribed burn
≥ 87	> 0.037	> 49	≥ 10	N/A	Thin, pileburn slash and fuels[6]
			< 10	N/A	Thin, pileburn slash
Mixed conifer wet (MCW) or mountain hemlock (MHD) plant associations					
< 87	N/A	N/A	N/A	N/A	Prescribed burn

[1]Stand Density Index, calculated in metric units (trees per ha).

[2]Crown bulk density (kg/m^3)

[3]Number of trees per hectare whose diameter at breast height (DBH) is less than 18 cm

[4]According to the Anderson rating system[4]

[5]Basal area in m^2 of all mountain hemlock (MHD) and white fir (WF) trees with DBH $> 46cm$.

[6]Pileburning slash involves removal of thinned trees only, while pileburning slash and fuels also involves removal of materials that were on the ground before thinning (Wall, Powers, 2012; personal communication)

≥ 87	> 0.037	> 49	$= 10$	> 7.5	Thin, pileburn slash and fuels, prescribed burn
			$= 10$	≤ 7.5	Thin, pileburn slash and fuels
			> 10	N/A	Thin, pileburn slash and fuels
			< 10	N/A	Thin, pileburn slash
		≤ 49	$= 10$	≥ 7.5	Prescribed burn
	≤ 0.037	N/A	$= 10$	≥ 7.5	Prescribed burn
	N/A	N/A	$\in \{6,8,9,10\}$	N/A	Prescribed burn[7]
Mixed conifer dry (MCD) plant association					
< 87	N/A	N/A	N/A	N/A	Prescribed burn
≥ 87	> 0.037	> 49	$\in \{10,11\}$	N/A	Thin, pileburn slash and fuels, prescribed burn
			≥ 12	N/A	Thin, pileburn slash and fuels
			< 10	N/A	Thin, pileburn slash
		≤ 49	$\in \{10,11\}$	N/A	Prescribed burn
	≤ 0.037	N/A	$\in \{10,11\}$	N/A	Prescribed burn
	N/A	N/A	$\in \{6,8,9,10\}$	N/A	Prescribed burn[7]

---

[7]Only if prescribed burn was assigned in period 1 (applies to period 2 treatment assignments only)
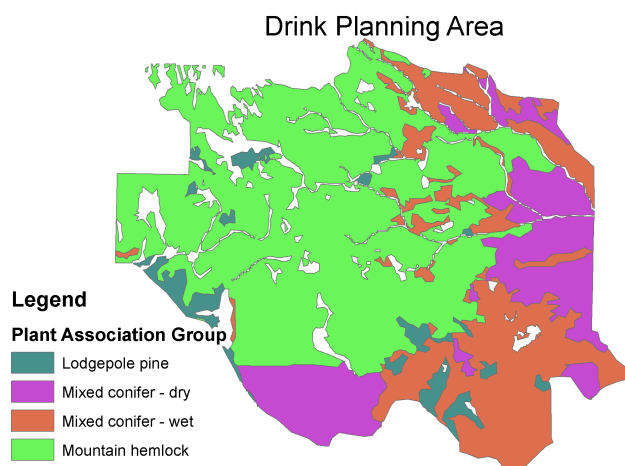
Figure B.1: Plant association groups in the Drink Area that are considered for treatments.

Appendix C

FRONTIER COMPARISON METRICS

This chapter describes in more detail metrics used to compare Pareto frontiers.

C.1 Dominance relations

Table C.1 defines the terms regarding dominance relations used here.

Relation	Solutions		Frontiers	
Strictly dominates	$\mathbf{z}^1 \succ\succ \mathbf{z}^2$	$\forall i \in \mathcal{M}, z_i^1 > z_i^2$	$Z^1 \succ\succ Z^2$	Every solution in Z^2 is strictly dominated by at least one solution in Z^1
Dominates	$\mathbf{z}^1 \succ \mathbf{z}^2$	$\forall i \in \mathcal{M}, z_i^1 \geq z_i^2 \wedge \exists i \in \mathcal{M}: z_i^1 > z_i^2$	$Z^1 \succ Z^2$	Every solution in Z_2 is dominated by at least one solution in Z_1
Better			$Z^1 \rhd Z^2$	Every solution in Z^2 is weakly dominated by at least one solution in Z^1 and $Z^1 \neq Z^2$
Weakly dominates	$\mathbf{z}^1 \succeq \mathbf{z}^2$	$\forall i \in \mathcal{M}, z_i^1 \geq z_i^2$	$Z^1 \succeq Z^2$	Every solution in Z^2 is weakly dominated by at least one solution in Z^1
Incomparable	$\mathbf{z}^1 \| \mathbf{z}^2$	Neither $\mathbf{z}^1$ nor $\mathbf{z}^2$ weakly dominates the other	$Z_1 \| Z_2$	Neither Z^1 nor Z^2 weakly dominates the other

Table C.1: Definitions of dominance relationships between solutions and between frontiers, reproduced from Zitzler *et al.* [84].

C.2   Additive binary epsilon indicator $I_{\epsilon+2}$

Given two frontiers, Z^1 and Z^2, the additive binary epsilon indicator is defined as in [84]:

$$I_{\epsilon+2}(Z^1, Z^2) = \inf_{\epsilon \in \mathbb{R}} \left\{ \forall \mathbf{z}^2 \in Z^2 \; \exists \mathbf{z}^1 \in Z^1 : \mathbf{z}^1 \succeq_{\epsilon_+} \mathbf{z}^2 \right\} \tag{C.1}$$

where $\succeq_{\epsilon_+}$ is the additive ϵ-dominance relationship:

$$\mathbf{z}^1 \succeq_{\epsilon_+} \mathbf{z}^2 \iff \epsilon + z_i^1 \geq z_i^2 \quad \forall 1 \leq i \leq M \tag{C.2}$$

Intuitively, ϵ is the minimum amount by which a frontier Z^1 must be translated such that every solution $\mathbf{z}^2 \in Z^2$ is "covered". See Figure C.1. Positive values of $I_{\epsilon+2}(Z^1, Z^2)$ indicate the presence of points $\mathbf{z}^2 \in Z^2$ that are not dominated by Z^1. Negative values of $I_{\epsilon+2}(Z^1, Z^2)$ indicate that Z^1 strictly dominates Z^2 ($Z^1 \succ\succ Z^2$).
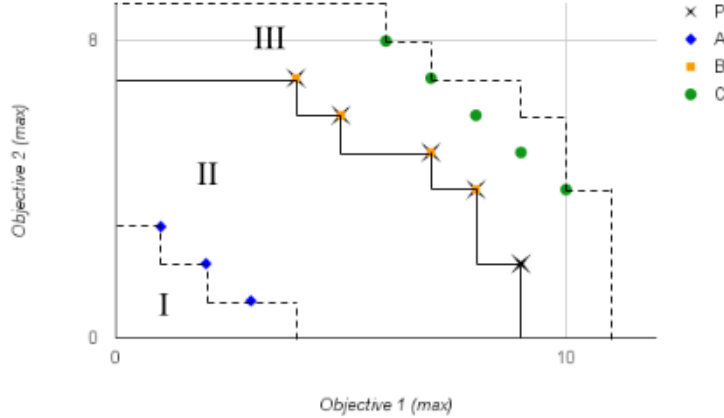

Figure C.1: Depiction of the additive binary epsilon indicator $I_{\epsilon+2}$ and the additive epsilon dominance relationship $\succeq_{\epsilon_+}$. In the figure,

$$I_{\epsilon+2}(P, A) = -4 < 0 \qquad I_{\epsilon+2}(P, B) = 0 \qquad I_{\epsilon+2}(P, C) = 2 > 0$$

Region III is ϵ_+-dominated for $\epsilon = 2$; region II is ϵ_+-dominated for $\epsilon = 0$; region I is ϵ_+-dominated for $\epsilon = -4$. Note that region II also encompasses region I, and region III encompasses region II.

C.3   Additive unary epsilon indicator I_{ϵ_+}

I define the unary epsilon indicator as

$$I_{\epsilon_+}(Z) = I_{\epsilon_+ 2}(Z, \mathbf{z}^{\text{ideal}}) \tag{C.3}$$

That is, the additive unary epsilon indicator is identical to the additive binary epsilon indicator where the second frontier consists of a single point: the ideal solution for the first frontier.

This differs from the unary epsilon indicator traditionally used in EMO [84] in which the frontier is compared against a reference nondominated set. However, because the frontiers in the present study have guaranteed optimality, there is no reference set against which to compare them.

C.4   Hypervolume Indicators

For every solution $\mathbf{z}^i$ in a frontier Z define the hyperrectangle r_i whose diagonal corners are the origin and the objective vector $\mathbf{z}^i = [z_1, \ldots, z_M]$ (see Figure C.2). Then the *unary hypervolume indicator* of the frontier Z is the M-dimensional volume of the union of all of the hyperrectangles corresponding to the solutions in Z:

$$I_{H1}(Z) = \text{vol} \left(\bigcup_{i=1}^{|Z|} r_i \right) \tag{C.4}$$

Then define the *binary hypervolume indicator* of two frontiers Z^1 and Z^2 as [83]

$$I_{H2}(Z^1, Z^2) = I_{H1}(Z^1 + Z^2) - I_{H1}(Z^2) \tag{C.5}$$

where $I_{H1}(Z^1 + Z^2)$ is the unary hypervolume indicator of the frontier consisting of the nondominated points in $Z = \{\mathbf{z} \in Z^1 \cup Z^2\}$. See Figure C.3. The binary hypervolume indicator provides the volume of frontier Z^1 that is not contained within frontier Z^2. Larger values of I_{H1} correspond to frontiers occupying larger amounts of the objective space.
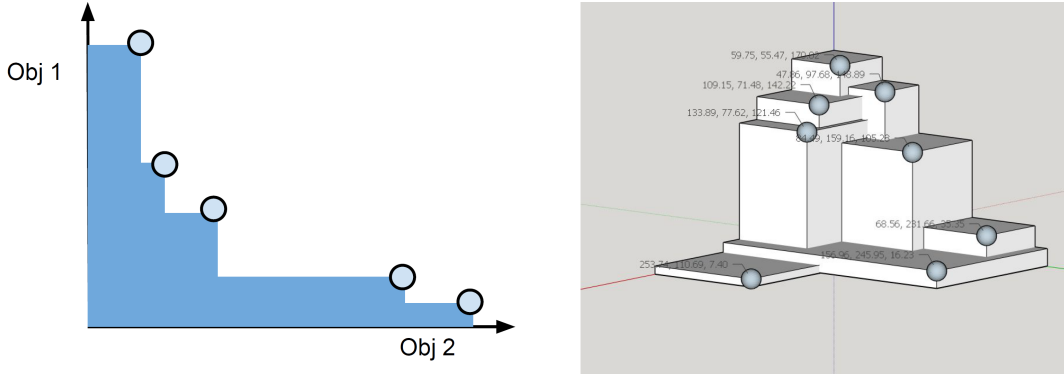
Figure C.2: Depiction of the hypervolumes of frontiers with two objectives (left) and three objectives (right).

$I_{H2}(Z^1, Z^2) > I_{H2}(Z^2, Z^1)$ indicates areas of less conflict between objectives in Z^1 than in Z^2.

I developed a custom algorithm to solve for the hypervolume indicators. The details of the algorithm may be found in §A.

C.5 Unary distance indicator I_d

The unary distance indicator measures the average distance from the frontier to the ideal solution:

$$I_d = \frac{1}{|Z|} \sum_{\mathbf{z} \in Z} ||\mathbf{z}^{\text{ideal}} - \mathbf{z}|| \tag{C.6}$$

Smaller values of I_d correspond to frontiers that are closer to the ideal solution, which may imply less conflict between objectives. This metric is analogous to the unary distance indicator more commonly used in EMO [19]. Where the metric used here measures the distance to the ideal solution, the traditional metric measures the distance to a reference Pareto frontier.
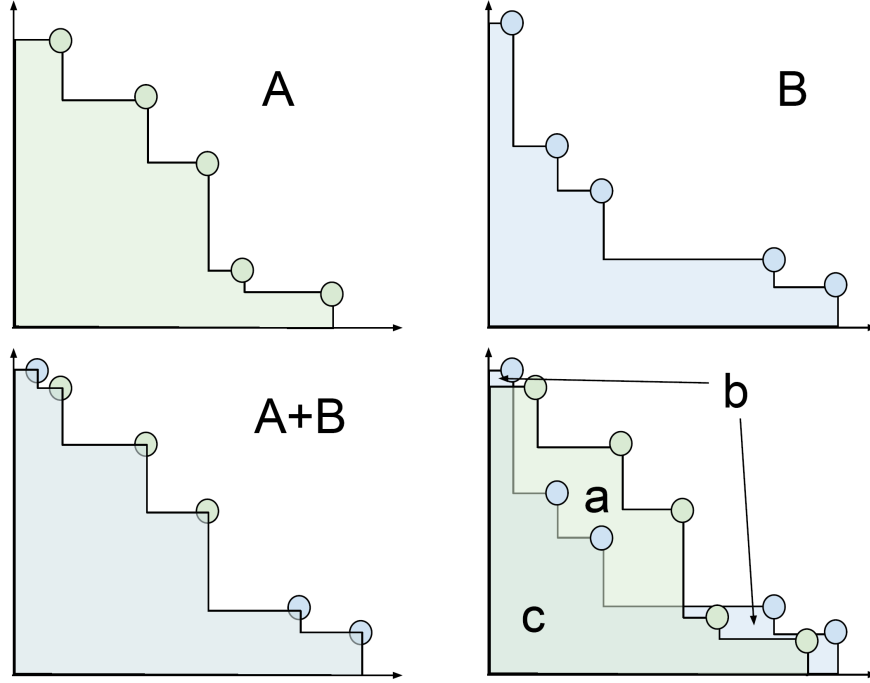
Figure C.3: Depiction of the binary hypervolume indicator. The individual frontiers are shown in the top row: frontier A (left) and frontier B (right). The merged frontier $A + B$ is shown in bottom left - note the absence of points that were dominated when combined. Following the naming of regions as shown in the bottom right figure, the binary hypervolume indicator is equal to

$$I_{H2}(A, B) = (\text{area}_a + \text{area}_b + \text{area}_c) - (\text{area}_b + \text{area}_c) = \text{area}_a$$

C.6 Unary Spacing Indicator I_s

The unary spacing indicator, or Schott's spacing metric [64], computes the standard deviation of the distance between points in the frontier:

$$I_s = \sqrt{\frac{1}{|Z| - 1} \sum_{\mathbf{z} \in Z} (d_z - \bar{d})^2} \tag{C.7}$$

where

$$d_z = \min_{\mathbf{y} \in Z, \mathbf{y} \neq \mathbf{z}} ||\mathbf{z} - \mathbf{y}|| \tag{C.8}$$

and $\bar{d}$ is the average over all d_z. In EMO, the spacing indicator provides a measure of an algorithm's ability to search the frontier space uniformly. Here, the spacing metric provides a measure of the flexibility afforded to the decision maker, since smaller values of I_s imply less distance between solutions.